UC Berkeley

Title

Role of the Coiled-Coil Domain in Allosteric Activity Regulation in Soluble Guanylate Cyclase.

Permalink

https://escholarship.org/uc/item/98m726kw

Journal

Biochemistry, 62(10)

Authors

Wittenborn, Elizabeth

Thomas, William

Houghton, Kimberly

et al.

Publication Date

2023-05-16

DOI

10.1021/acs.biochem.3c00052

Peer reviewed

Role of the coiled-coil domain in allosteric activity regulation in soluble guanylate cyclase

Elizabeth C. Wittenborn[1,†], **William C. Thomas**[1,†], **Kimberly A. Houghton**[2], **Erika S. Wirachman**[3,§], **Yang Wu**[2], **Michael A. Marletta**[1,2,3,*]

[1]California Institute for Quantitative Biosciences, University of California, Berkeley, Berkeley, CA 94720, USA

[2]Department of Chemistry, University of California, Berkeley, Berkeley, CA 94720, USA

[3]Department of Molecular and Cell Biology, University of California, Berkeley, Berkeley, CA 94720, USA

Abstract

Soluble guanylate cyclase (sGC) is the primary nitric oxide (NO) receptor in higher eukaryotes, including humans. NO-dependent signaling via sGC is associated with important physiological effects in the vascular, pulmonary, and neurological systems, and sGC itself is an established drug target for the treatment of pulmonary hypertension due to its central role in vasodilation. Despite isolation in the late 1970s, high-resolution structural information on full-length sGC remained elusive until recent cryo-electron microscopy structures were determined of the protein in both the basal unactivated state and the NO-activated state. These structures revealed large-scale conformational changes upon activation that appear to be centered on rearrangements within the coiled-coil (CC) domains in the enzyme. Here, a structure-guided approach was used to engineer constitutively unactivated and constitutively activated sGC variants through mutagenesis of the CC domains. These results demonstrate that the activation-induced conformational change in the CC domains is necessary and sufficient for determining the level of sGC activity.

Graphical Abstract

*To whom correspondence may be addressed: Michael A. Marletta: marletta@berkeley.edu.
§Current address: Department of Biology, Massachusetts Institute of Technology, Cambridge, MA 02139, USA
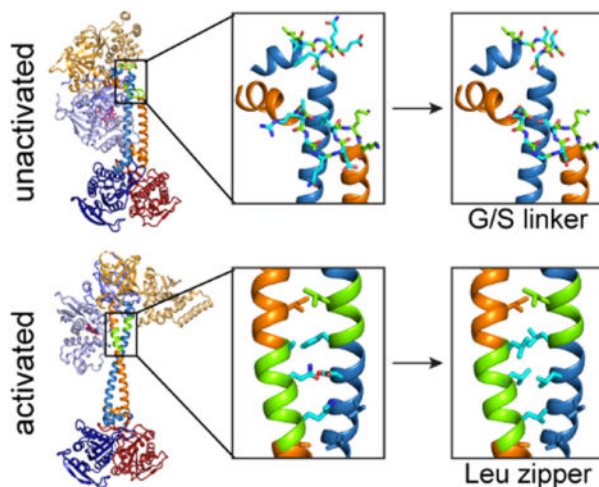†Equal contributions

Nitric oxide (NO) is a freely diffusible, biological signaling molecule that plays a variety of physiological roles across domains of life, and in humans and other higher eukaryotes NO is involved in regulating vasodilation, platelet aggregation, and neurotransmission.[1–7] The central NO receptor in these processes is the enzyme soluble guanylate cyclase (sGC), which catalyzes the conversion of guanosine triphosphate (GTP) to the secondary messenger cyclic guanosine monophosphate (cGMP).[8] cGMP regulates the activity of downstream effectors, including kinases, ion channels, and phosphodiesterases, leading to the physiological responses mentioned above. Defects in this NO-dependent signaling pathway are associated with several disease pathologies, and sGC has proven to be a successful drug target for the treatment of pulmonary hypertension through the action of small molecular stimulators such as the drug riociguat (Adempas®), which was approved by the US FDA in 2013.[9]

sGC is a heme-containing enzyme that exhibits an NO-dependent increase in specific activity. Most studies report on the increase in activity from the unliganded (basal) state to that observed after treatment of the enzyme with an excess of NO (excess-NO). Others have investigated the changes in activity observed between 1) the unliganded state, 2) a state containing a single molar equivalent of NO relative to the heme concentration (1-NO), and 3) the excess-NO state.[10–12] Of further note, the activity observed between the 1-NO state and the excess-NO state is freely reversible, leading us to speculate that these two forms are important physiological contributors to activity.[11,12] A single molar equivalent of NO (1-NO) leads to a relatively modest ~4–5–fold increase in activity, while the presence of a molar excess of NO (excess-NO) results in an additional ~5–50–fold increase over the 1-NO activity level.[10–13] In the 1-NO state, NO binds to the heme cofactor forming a five-coordinate Fe^{2+}–NO adduct,[14,15] and this ligation state is maintained upon addition of excess NO. The mechanism of further activation is unknown, although it has been suggested that cysteine residues may play a role in conferring maximal activity in the excess-NO state.[12,16] Notably, the 1-NO state has been suggested to be the physiological resting state of sGC based on estimates of the K_d for NO from the heme (low pM range)[17] and the intracellular NO concentration (100–5000 pM).[18] Thus, in cells, sGC likely cycles between the 1-NO and excess-NO states. In addition to the presence of excess NO, high activity can also be attained, both *in vitro* and *in vivo*, by addition of small molecule stimulators such as

the benzylindazol derivative YC-1 to the 1-NO state of sGC.[12,19,20] Indeed, YC-1 has served as the starting point for development of sGC-targeted drugs, including riociguat.[9,21–24]

sGC is heterodimeric and composed of homologous α and β subunits that each contain four distinct domains: an N-terminal heme nitric oxide/oxygen binding (H-NOX) domain, a Per-Arnt-Sim (PAS) domain, a coiled-coil (CC) domain, and a C-terminal catalytic (CAT) domain. Despite this homology, only the β H-NOX domain binds a heme cofactor and is the site which binds the first equivalent of NO.[25–28] The α H-NOX domain contains an N-terminal extension that partially occupies the heme binding site, prohibiting heme incorporation.[29] The overall structure and domain arrangement of sGC has been revealed by single-particle cryo-electron microscopy (EM).[29–31] The protein is an elongated particle consisting of two distinct lobes connected by a stalk-like density. The larger of the two lobes contains a central α/β PAS dimer flanked by the two H-NOX domains and has been termed the regulatory lobe.[29–31] The stalk-like connector region contains the CC domains and connects to the smaller globular lobe, which contains the α/β CAT dimer and has thus been termed the catalytic lobe.[29–31] Recent, high-resolution cryo-EM structures of sGC from *Homo sapiens* (*Hs*, human) and *Manduca sexta* (*Ms*, tobacco hawk moth) revealed dramatic conformational changes that take place upon enzyme activation (Figure 1).[29,30] In the unliganded, unactivated state, sGC adopts a contracted conformation that appears to be achieved through an unexpected bending of the CC domains (highlighted in green in Figure 1). Upon activation, the protein extends, and the regulatory lobe rotates ~70° relative to the catalytic lobe (Figure 1). In the activated state, the portions of the CC domains that were bent in the unactivated state straighten to form two long helices that extend from the PAS dimer to the CAT dimer (Figure 1). This large-scale conformational change is coupled to rearrangements in the CAT domains that open up the active site to allow for GTP binding.[29,30]

Given that there is no direct contact between the N-terminal regulatory lobe and the C-terminal catalytic lobe, straightening of the CC domains appears to be a critical contributor to allosteric communication through the protein. In one of the cryo-EM studies, constitutive breaks in one or the other of the CC helices were engineered by the introduction of proline residues (α-D423P or β-G356P) in the bent region of the unactivated *Hs* sGC CCs.[29] NO-dependent activation was severely impaired in both variants, although the activity of the α-D423P variant in the activated, excess-NO state still more than doubled relative to the unliganded, unactivated state.[29] These observations are consistent with independent mutagenesis and molecular dynamics simulations, which had suggested crosstalk between the CC domains and both the β H-NOX and CAT domains, respectively.[32,33]

The EM analysis of *Ms* sGC revealed an interesting connection between the CC conformation and the sGC stimulator YC-1. YC-1 was included in the EM sample along with excess-NO to stabilize the fully activated conformation of the protein.[30] Electron density consistent with the size and shape of YC-1 was observed between the β H-NOX and α CC domains in the structure of activated *Ms* sGC.[30] This structure and ensuing higher resolution structures of *Hs* sGC with YC-1[34] revealed that the YC-1 density is adjacent to the region of the α CC domain that is bent in the unactivated state.[34,35] This observation underscores the importance of the CC domains in sGC activity, and it has been proposed

that the mechanism of YC-1 and related stimulators might be to stabilize the straightened conformation of the CC domains.[34,35] Indeed, YC-1 has been shown to have only a minimal effect on the unliganded, unactivated state of sGC, whereas it stimulates the 1-NO state to a high level of activity.[12,20,30] The 1-NO state is thought to exist as an equilibrium between the bent, unactivated conformation of sGC and a partially extended conformation,[30] and YC-1 may serve to shift this equilibrium by initially binding to the partially extended state and stabilizing it in the fully extended state.

To provide further insight into the role of the CC domains in the activation mechanism of sGC, we have used structure-guided mutagenesis within these domains of *Ms* sGC to generate 1) sGC variants with constitutively unstraightened CC domains, and 2) an sGC variant with constitutively straight CC domains. The activity profiles of these variants have been measured under different ligation states—unliganded, 1-NO, excess-NO, and 1-NO + YC-1—to determine the effect of CC conformation on sGC activity.

Materials and Methods

Mutagenesis and generation of expression constructs.

Wild-type (WT) *Ms* sGC constructs were generated previously in the pFastBac vector (Bac-to-Bac Baculovirus Expression System) and were termed pFastBac_Ms_sGC_α1_His6 and pFastBac_Ms_sGC_β1 for the α and β subunits, respectively.[30] The α subunit gene was appended with the sequence for a C-terminal hexa-histidine tag. In the present work, mutagenesis was performed by PCR to generate mutant gene fragments, which were then re-cloned into the linearized pFastBac vector using Gibson assembly. Constructs were validated by Sanger sequencing at the UC Berkeley DNA Sequencing Facility.

Plasmids were transformed into DH10Bac-GFP *E. coli* cells to allow for transposition into baculovirus bacmids. Bacmids were isolated from successful transposants and the sGC genes were amplified by PCR and sequenced for validation. Bacmids were then transfected into Sf9 insect cells to generate recombinant baculoviruses. Baculoviruses containing the α and β subunits were amplified separately on 300-mL scales prior to co-infection for protein expression cultures.

Variant structure prediction.

For all three constructs, structural prediction was performed using AlphaFold2[36] via ColabFold.[37] 5-rank default model parameters were used with a template date cutoff of July 7, 2022. No major differences were observed between models of different rank in structured regions, and so unrelaxed rank 1 models were subsequently analyzed for each variant. Prediction confidence (pLDDT score) was used as a tool for assessing potential structural stabilization or destabilization.

Protein expression and purification.

Protein was expressed in Sf9 insect cells at 27 °C with shaking at 130 rpm. Sf9 cultures were infected with 50 mL/L of amplified α and β viruses (100 mL of total virus per L) and

grown for 72 h. Cells were harvested by centrifugation at $4300 \times g$ for 20 min, flash frozen in liquid nitrogen (LN2), and stored at −80 °C.

Protein was purified as described previously.[30] All steps were performed at 4 °C, unless otherwise noted. Briefly, cell pellets were thawed in a room temperature water bath and resuspended in Buffer A (50 mM K_2HPO_4, 200 mM NaCl, 1 mM imidazole, 1 mM benzamidine, 5% (v/v) glycerol, 5 mM β-mercaptoethanol, pH 8) supplemented with 10 mM benzamidine, 1 mM AEBSF, 0.5 mM DNase I. Cells were lysed by 3 rounds of bead beating for 20 s intervals with 1 min rests in between. Beads were removed by centrifugation at $2800 \times g$ for 5 min. Lysate was clarified by centrifugation at $158000 \times g$ for 2 h. Lysate was applied to a 2-mL TALON superflow column at 0.5 mL/min using a BioLogic LP low-pressure chromatography system. The column was washed with 20 column volumes (CV) Buffer A. Protein was eluted with 10 CV Buffer B (50 mM K_2HPO_4, 200 mM NaCl, 125 mM imidazole, 1 mM benzamidine, 5% (v/v) glycerol, 5 mM β-mercaptoethanol, pH 8) and 2-mL fractions were collected. Fractions containing sGC were concentrated to < 1 mL, supplemented with 5 mM DTT and 1 mM EDTA, and stored on ice at 4 °C overnight. The sample was then diluted to 10 mL with Buffer C (25 mM triethanolamine (TEA), 25 mM NaCl, 5% (v/v) glycerol, 5 mM DTT, pH 7.4) and applied to a POROS HQ2 anion exchange column at 0.5 mL/min using an ÄKTA pure chromatography system. The column was washed with 3 CV Buffer C and then a gradient up to 50% Buffer D (25 mM TEA, 750 mM NaCl, 5% (v/v) glycerol, 5 mM DTT, pH 7.4) was developed over 17 CV. Fractions were analyzed by SDS-PAGE and those containing purified sGC were concentrated, drop frozen in LN2, and stored in LN2.

Activity assays and cGMP quantification.

Samples were handled inside of a Coy anaerobic chamber. Protein was thawed at 4 °C, incubated with 10 mM sodium dithionite for 15 min to fully reduce the heme cofactor, and then desalted over a Zeba spin desalting column pre-equilibrated with Buffer E (50 mM HEPES, 150 mM NaCl, 5% glycerol, pH 7.5). Ultraviolet-visible (UV-Vis) absorption spectra of the unliganded sample were recorded using a NanoDrop 2000C microvolume spectrophotometer. The protein concentration was determined using the Soret peak of the reduced heme (λ_{max} = 433 nm, ε_{434} = 149000 $M^{-1}cm^{-1}$).[30,38] An aliquot of unliganded protein was reserved for the activity assay. To the remaining protein, Proli-NONOate was spiked in (0.75 μL 30 mM Proli-NONOate added to ~30 μL samples; ~1 mM Proli-NONOate working concentration) to generate the excess-NO state and UV-Vis spectra were recorded. The concentration of the excess-NO state was assumed to be nominally the same as the unliganded state. Protein was then desalted into Buffer E to obtain the 1-NO state and UV-Vis spectra were recorded. The concentration of the 1-NO state was determined by comparison of the A_{399} Soret peak of the Fe^{2+}–NO species to that of the excess-NO sample.

Activity assays were conducted at 25 °C in Buffer E supplemented with 5 mM DTT and 3 mM $MgCl_2$. Assays were conducted at enzyme concentrations of 20, 30, or 10 nM holo protein for the WT, GSG, and Leu zipper variants, respectively. YC-1 (150 μM) or Proli-NONOate (150 μM) were added as necessary to generate the 1-NO + YC-1 and excess-NO states, respectively. Reactions were initiated by addition of 1.5 mM GTP and

timepoints were quenched 1:4 (v:v) into 125 mM zinc acetate. The pH of the quenched reaction samples was then adjusted by addition of an equal volume of 125 mM sodium carbonate. Samples were stored at −80 °C.

Quenched assay samples were thawed at room temperature and the zinc precipitate was removed by centrifugation at $30,130 \times g$ for 5 minutes at room temperature. Samples were diluted and cGMP was quantified using a cGMP enzyme-linked immunosorbent assay (ELISA) following the manufacturer's instructions (Enzo Life Sciences). Initial rates were calculated from the linear regions of the time course where <10% of the GTP substrate was consumed.

Small-angle X-ray Scattering

Small-angle X-ray scattering (SAXS) was performed under anaerobic conditions on *Ms* sGC(GSG2) at the MacChess BioSAXS beamline (Sector 7B) at the Cornell High-Energy Synchrotron Source, Ithaca, New York.[39,40] 30 μL of sGC was reduced in an anaerobic glovebox, then exchanged into SAXS assay buffer (50 mM HEPES pH 7.5, 150 mM NaCl, 1% glycerol, 1 mM TCEP). After confirming heme reduction via UV/vis spectrophotometry, 40 μL of 3.9 μM sample was injected directly into an anaerobic flow cell operating in batch mode. Data were collected using a Dectris PILATUS3 × 2M detector at 4 °C. 20 × 1s X-ray exposures were collected. Scattering images were integrated about the beam center and normalized by transmitted intensities measured on a photodiode beamstop. The integrated protein scattering profile, $I(q)$, was produced by subtraction of background buffer scattering from the protein solution scattering using an exact buffer match. The X-ray wavelength was set at $\lambda = 1.1018$ Å and the sample-to-detector distance was 1713 mm, as determined by silver behenate calibration. Scattering was collected over a range of $q = 0.01$ Å^{-1} to 0.48 Å^{-1}, where q is the scattering vector $q = 4\pi\sin\theta/\lambda$ and 2θ is the scattering angle. Data processing, analysis, and comparison to published WT *Ms* sGC[31] were performed in BioXTAS RAW using established protocol.[41] Radii of gyration (R_g) were estimated with Guinier analysis, and pair distance distribution analysis was performed in GNOM.[42] Error bars associated with R_g values are curve-fitting uncertainties from Guinier analysis. The predicted scattering of unactivated WT *Ms* sGC was calculated from the experimental unactivated structure PDB ID 6PAS using Crysol.[42] Difference scattering was calculated in Primus.[42]

Results and Discussion

Constitutively unactivated sGC variants.

The bent regions of the CC domains in *Ms* sGC are residues α-420–426 (sequence: ARAQDGL) and β-346–350 (sequence: MSEQF). To generate sGC variants with constitutively unstraightened CC domains these residues were replaced with glycine-serine (GS) repeats. Such GS repeats are widely used as linkers in recombinant protein engineering to spatially separate functional regions of a protein construct, and are chosen due to their inherent conformational flexibility.[43–45] Thus, we hypothesized that substitution of the native sequences in the bent regions of the CCs with GS repeats would prevent secondary structure formation and straightening of the CCs. Two *Ms* sGC α constructs were made,

one in which the entire bent region was replaced (ARAQDGL → GSGGSGS) and the other, a more conservative construct, in which only part of this region was altered (AR<u>AQD</u>GL → AR<u>GSG</u>GL, changes underlined). A single *Ms* sGC β construct was used in which the entire region was changed (MSEQF → GSGSG). Two final protein variants were made using these constructs: the variant containing α—GSGGSGS/β-GSGSG will be referred to as *Ms* sGC(GSG1), and that containing α—GSG/β-GSGSG is termed *Ms* sGC(GSG2). AlphaFold2 models were determined for WT *Ms* sGC and both GSG variants to help predict structural characteristics.[36,37] Although a WT experimental structure exists,[30] a prediction was produced for comparative analysis. For WT and both variants, AlphaFold2 predicts an activated, straightened CC conformation that is similar to experimental structures (Figure S1A–C). For the GSG variants, however, the residues in and around the mutated region exhibit decreased predictive confidence scores (pLDDT), particularly for the GSG1 variant, suggesting a lower propensity for the predicted secondary structure (Figure S1A–C, Table S1). While AlphaFold2 is not designed to be predictive of structural changes induced by site-directed mutagenesis,[46] the lower pLDDT in the GSG variants suggests a shift away from structural elements found in stable CC domains in the AlphaFold2 training dataset, i.e., in experimental structures of CC domains. Thus, the results of this prediction support the destabilizing effect expected from engineering GS repeats into the CC domain.

Both GSG variants co-purify as two bands of relatively equal intensity by SDS-PAGE, indicative of heterodimer formation (Figure S2A,B). They also exhibit UV-Vis absorption spectra with Soret maxima at 433 nm for the Fe^{2+} unliganded species, as reported previously for wild-type (WT) *Ms* sGC (Figure 2A,B).[30,38] Unlike the WT protein, a shoulder on the Soret band centered at ~426 nm is also apparent in both spectra (Figure 2A,B). The cause of this shoulder is unknown, although a Soret band at 426 nm has been previously reported for reconstituted human sGC[47] and for truncations of rat sGC[27]. The ratio of absorbances at 433 nm and 280 nm was used to estimate the heme incorporation for each variant relative to that observed for the WT enzyme. For typical preparations of WT *Ms* sGC, $A_{433}/A_{280} = 0.85$.[30] This ratio is 0.47 and 0.64 for *Ms* sGC(GSG1) and *Ms* sGC(GSG2), respectively, reflecting heme incorporations of ~55% and 75% of WT levels, respectively. The Soret maxima of the variants shift to 399 nm upon NO binding, consistent with formation of the five-coordinate Fe^{2+}–NO species (Figure 2A,B).[14,15,30,38]

The activity of both variants is low (Figure 2C, Figure S3). Importantly, no increase in activity is observed with any amount of added NO, suggesting that even the activity of the 1-NO state is dependent on straightening of the CC domains. This idea is consistent with previous analysis of the 1-NO state by small angle X-ray scattering (SAXS), which suggested that the 1-NO state exists as a conformational equilibrium that is best described as a mixture of the bent, unactivated conformation (72% of the population) and a partially extended conformation (28% of the population).[30] In this scenario, the activity of the 1-NO state would arise from the fraction of the sample that adopts the partially extended conformation, and when this conformation cannot be accessed, as in the *Ms* sGC(GSG1) and *Ms* sGC(GSG2) variants, the activity of the protein remains low. These results are also consistent with the previously reported activities of the α-D423P and β-G356P variants of *Hs* sGC.[29] Also notable is that YC-1 does not stimulate activity in the variants. Though it is possible that the mutations made abolish YC-1 binding entirely, there is no structural

evidence that the mutated residues are directly associated with YC-1 binding.[30,34] Instead, lack of YC-1 stimulation is more consistent with the hypothesis that YC-1 interacts with and stabilizes the already straightened conformation of the α CC and that the CC domains in the variants are incapable of sampling an unbent conformation.

An alternative explanation for low activity of *Ms* sGC(GSG1) and *Ms* sGC(GSG2) is that these variants are improperly folded or cannot dimerize properly. To test this possibility, SAXS was performed on *Ms* sGC(GSG2). SAXS is a structural technique that can be performed on a protein in solution and provides information about folding, oligomeric state, and conformational state. Sample quality and quantity limitations prevented a similar experiment on *Ms* sGC(GSG1). SAXS was performed anaerobically after the protein was reduced to the ferrous oxidation state of the heme. The SAXS profile of *Ms* sGC(GSG2) was collected without ligand bound and directly compared to that of WT *Ms* sGC reported in a previous study[30] (Figure 3A–B). Sample quantity prevented the use of size-exclusion-coupled chromatography SAXS (SEC-SAXS) as was previously performed for WT *Ms* sGC, and so the experimental profile shows a lower signal-to-noise scattering ratio. There is also evidence of aggregation at low *q*-value as compared to the previous study, a characteristic similarly observed in handling of WT *Ms* sGC. The aggregation component of the solution contributes to an inflated radius of gyration (R_g) for sGC(GSG2) of 54.5 ± 0.3 Å compared with 43.1 ± 0.4 for WT sGC.[30] Nonetheless, when normalized by their overall scattering intensity, the scattering of *Ms* sGC(GSG2) and WT *Ms* sGC without NO present are close matches in the mid-*q* and high-*q* regimes (Figure 3C). Likewise, the scattering of *Ms* sGC(GSG2) matches the calculated scattering of the unactivated WT *Ms* sGC (PDB ID 6PAS, Figure 3A–B, black dotted). The similarity of the scattering profiles is strong evidence that most *Ms* sGC(GSG2) in solution is folded and forms a heterodimer of a similar conformation to unactivated WT sGC. By contrast, 1-NO sGC in a partially extended conformational state was previously found to display a pronounced increase in mid-*q* scattering at ~0.07 Å^{-1} not seen in *Ms* sGC(GSG2) (Figure 3B–C, pink). Thus, the SAXS experiment supports the conclusion that *Ms* sGC GS-linker mutants are properly folded but trapped in an unactivated conformation of the protein.

Constitutively activated sGC variant.

Recent EM analysis of sGC revealed an NO-dependent conformational change centered on straightening of the CC domains. This straightening of the CCs leads to repacking of the two CC helices such that the CAT domains open to allow for GTP binding and subsequent hydrolysis.[29,30,34] Thus, to generate a constitutively activated sGC variant, we sought to stabilize the straightened conformation of the CCs. Residues along the dimer interface of the activated, straightened portion of the CC domains were changed to leucine residues to generate a leucine zipper-like motif. Leucine zippers are common structural motifs in proteins in which amphipathic α-helices dimerize via hydrophobic interactions.[48,49] Sequences of leucine zippers are typified by heptads in which every seventh residue is a leucine. These leucine residues then form the hydrophobic core of the coiled coil "zipper". We hypothesized that we could stabilize the secondary structure of the sGC CC domains in a straightened conformation by the selective introduction of leucine residues. The residue substitutions made are: α-A420L, α-Q423L, α-R427L, β-F350L, and β-D353L; this variant

will be referred to as *Ms* sGC(Leu zipper). An AlphaFold2 model was also determined for the Leu zipper variant. AlphaFold2 predicts the activated, straightened CC conformation and has an increased confidence score (pLDDT) for residues in and around the mutated CC-domain interface relative to WT, suggesting a higher likelihood for the straightened conformation (Figure S1D, Table S1).

Ms sGC(Leu zipper) co-purifies as two bands by SDS-PAGE, indicative of heterodimer formation (Figure S2C). It was isolated with ~41% heme incorporation relative to WT, based on an A_{433}/A_{280} ratio of 0.35 (Figure 4A). The reduced variant exhibits a UV-Vis Soret maximum at 433 nm, with a slight shoulder at 426 nm, that shifts to 399 nm upon NO binding (Figure 4A). The activity of the variant is constitutively high and independent of ligation state (Figure 4B). The lack of activation by YC-1 suggests that the protein is already stabilized in the fully activated state through the introduction of the leucine zipper motif. Interestingly, when the specific activity of *Ms* sGC(Leu zipper) is calculated per milligram of holo protein, with the protein concentration estimated from the Soret absorbance at 433 nm, the activity appears unusually high (~4000 nmol cGMP/min/mg sGC) (Figure S4). One explanation for this observation may be that the heme-containing variant, even under basal conditions, supports higher activity than the heme-containing WT under excess-NO conditions due to the increased rigidity of the straightened CC domains. Alternatively, the apo variant may itself have high activity. When the total protein concentration, accounting for the 59% apo protein in the sample, is used to calculate the specific activity, the values are similar to those observed for the WT protein (~1500 nmol cGMP/min/mg sGC) (Figure 4B, Figure S4). Thus, introduction of the leucine zipper motif may also exert an effect on the apo protein, rendering it constitutively active, as well.

We were unable to obtain quantities of *Ms* sGC(Leu zipper) sufficient to determine its structure by SAXS. However, heightened constitutive activity is challenging to explain by misfolding or mis-oligomerization. Instead, the combination of our biochemical data suggests that the most likely explanation for activity increase is that the mutations to the CC-domain stabilize the active conformation.

Heme-deficient WT Ms sGC.

The three *Ms* sGC CC variants described here were found to have a lower heme content than typical preparations of the WT enzyme. To determine whether the presence of apo protein in the samples affected the observed activity profiles of the variants, we sought to obtain samples of WT *Ms* sGC with low heme incorporation. It is well known that the sGC heme dissociates more readily in the Fe^{3+} oxidized state than in the Fe^{2+} reduced state.[50,51] Therefore, to promote oxidation and subsequent heme loss, less reducing agent was used during the course of the purification. In particular, DTT was not added to the sample between the affinity and anion exchange chromatography steps, allowing for oxidation to occur during the overnight storage period between the two columns (see Methods). Following purification, the protein was reduced with sodium dithionite and the UV-Vis spectrum was recorded to assess the resulting heme content (Figure 5A). The A_{433}/A_{280} ratio of the reduced protein was 0.33, in contrast to the typical ratio of 0.85 for WT *Ms* sGC,[30] indicating a heme content of ~39%, relative to typical preparations of WT. The

39% holo WT protein exhibits a standard three-state activity profile, confirming that the background of apo protein does not measurably affect the relative, ligation state–dependent activity states of sGC (Figure 5B). Additionally, the specific activities obtained for this protein are comparable to those of typical, heme-replete WT *Ms* sGC,[30] further suggesting that the presence of apo protein in our variant samples should not have a significant effect on the interpretation of the data.

Conclusions

Recent high-resolution cryo-EM structures of sGC in the unactivated and activated states revealed large-scale, ligand-induced conformational changes, providing an initial structural basis for understanding allostery in this important enzyme.[29,30,34] In particular, the structures indicate that rearrangements in the CC domains may play an important role in intramolecular signal transduction: the CC domains are bent in the unactivated state and then straighten to form two long, continuous helices upon activation. Furthermore, the structures reveal an association between the straightened α CC domain and the small molecule stimulator YC-1, suggesting that this class of molecules might function by stabilizing the straightened, activated conformation of sGC. To provide insight into the significance of the sGC conformational change, structure-guided protein engineering within the CC domains has been used to generate variants with constitutively unstraightened CCs and constitutively straight CCs. To prevent CC straightening, flexible GS linker-like regions were incorporated into the bent portion of the unactivated CCs. These variants retain a basal level of activity regardless of ligation state, highlighting the functional relevance of these domains in activation. A SAXS experiment provides further evidence that this basal activity is a result of folded, dimeric protein trapped in a conformation that closely resembles that of unactivated WT sGC.

To promote formation of constitutively straight CCs, a leucine zipper motif was engineered into the CC dimer interface of the activated conformation. The leucine zipper variant exhibits constitutively high levels of activity, indicating that stabilization of the straightened CCs does indeed promote activation. Throughout our investigations, sGC activity variants expressed poorly via insect cells and with reduced heme incorporation, creating significant hurdles to structural and biochemical analysis. Indeed, we hypothesize that the leucine zipper variant's particularly poor expression may be because its constitutive cyclase activity is toxic to insect cells. However, the design principles used for these activity variants can be extended to sGCs from other organisms and expression systems, creating an opportunity for future work utilizing engineered activity variant orthologs to better understand sGC structure and activation.

This work represents an important structure-based investigation of allostery in sGC and suggests that straightening of the CC domains is necessary and sufficient for full enzyme activation. Additionally, the lack of activation by YC-1 in any of the variants supports the hypothesis that YC-1 binds to and stabilizes the straightened conformation of the α CC domain, a finding that may aid in the development of new sGC-targeted drugs.

Supplementary Material

Refer to Web version on PubMed Central for supplementary material.

Acknowledgements

Funding

References

(1). Bohlen HG Nitric Oxide and the Cardiovascular System. Compr. Physiol 2015, 5, 803–828. 10.1002/cphy.c140052.

(2). Steinert JR; Chernova T; Forsythe ID Nitric Oxide Signaling in Brain Function, Dysfunction, and Dementia. The Neuroscientist 2010, 16 (4), 435–452. 10.1177/1073858410366481. [PubMed: 20817920]

(3). Buys E; Sips P New Insights into the Role of Soluble Guanylate Cyclase in Blood Pressure Regulation. Curr. Opin. Nephrol. Hypertens 2014, 23 (2), 135–142. 10.1097/01.mnh.0000441048.91041.3a. [PubMed: 24419369]

(4). Stasch Johannes-Peter; Pacher Pál; Evgenov Oleg V. Soluble Guanylate Cyclase as an Emerging Therapeutic Target in Cardiopulmonary Disease. Circulation 2011, 123 (20), 2263–2273. 10.1161/CIRCULATIONAHA.110.981738. [PubMed: 21606405]

(5). Ben Aissa M; H. Lee S; M. Bennett B; R.J. Thatcher G Targeting NO/CGMP Signaling in the CNS for Neurodegeneration and Alzheimer's Disease. Curr. Med. Chem 2016, 23 (24), 2770–2788. 10.2174/0929867323666160812145454. [PubMed: 27776476]

(6). Ghosh A; Koziol-White CJ; Asosingh K; Cheng G; Ruple L; Groneberg D; Friebe A; Comhair SAA; Stasch J-P; Panettieri RA; Aronica MA; Erzurum SC; Stuehr DJ Soluble Guanylate Cyclase as an Alternative Target for Bronchodilator Therapy in Asthma. Proc. Natl. Acad. Sci 2016, 113 (17), E2355–E2362. 10.1073/pnas.1524398113. [PubMed: 27071111]

(7). Papapetropoulos A; Simoes DCM; Xanthou G; Roussos C; Gratziou C Soluble Guanylyl Cyclase Expression Is Reduced in Allergic Asthma. Am. J. Physiol.-Lung Cell. Mol. Physiol 2006, 290 (1), L179–L184. 10.1152/ajplung.00330.2005. [PubMed: 16143586]

(8). Arnold WP; Mittal CK; Katsuki S; Murad F Nitric Oxide Activates Guanylate Cyclase and Increases Guanosine 3':5'-Cyclic Monophosphate Levels in Various Tissue Preparations. Proc. Natl. Acad. Sci 1977, 74 (8), 3203–3207. 10.1073/pnas.74.8.3203. [PubMed: 20623]

(9). Conole D; Scott LJ Riociguat: First Global Approval. Drugs 2013, 73 (17), 1967–1975. 10.1007/s40265-013-0149-5. [PubMed: 24218053]

(10). Russwurm M; Koesling D NO Activation of Guanylyl Cyclase. EMBO J. 2004, 23 (22), 4443–4450. 10.1038/sj.emboj.7600422. [PubMed: 15510222]

(11). Cary SPL; Winger JA; Marletta MA Tonic and Acute Nitric Oxide Signaling through Soluble Guanylate Cyclase Is Mediated by Nonheme Nitric Oxide, ATP, and GTP. Proc. Natl. Acad. Sci 2005, 102 (37), 13064–13069. 10.1073/pnas.0506289102. [PubMed: 16131543]

(12). Fernhoff NB; Derbyshire ER; Marletta MA A Nitric Oxide/Cysteine Interaction Mediates the Activation of Soluble Guanylate Cyclase. Proc. Natl. Acad. Sci 2009, 106 (51), 21602–21607. 10.1073/pnas.0911083106. [PubMed: 20007374]

(13). Emmons TL; Mathis KJ; Shuck ME; Reitz BA; Curran DF; Walker MC; Leone JW; Day JE; Bienkowski MJ; Fischer HD; Tomasselli AG Purification and Characterization of Recombinant Human Soluble Guanylate Cyclase Produced from Baculovirus-Infected Insect Cells. Protein Expr. Purif 2009, 65 (2), 133–139. 10.1016/j.pep.2009.01.001. [PubMed: 19189860]

(14). Gerzer R; Böhme E; Hofmann F; Schultz G Soluble Guanylate Cyclase Purified from Bovine Lung Contains Heme and Copper. FEBS Lett. 1981, 132 (1), 71–74. 10.1016/0014-5793(81)80429-2. [PubMed: 6117479]

(15). Stone JR; Marletta MA Soluble Guanylate Cyclase from Bovine Lung: Activation with Nitric Oxide and Carbon Monoxide and Spectral Characterization of the Ferrous and Ferric States. Biochemistry 1994, 33 (18), 5636–5640. 10.1021/bi00184a036. [PubMed: 7910035]

(16). Alapa M; Cui C; Shu P; Li H; Kholodovych V; Beuve A Selective Cysteines Oxidation in Soluble Guanylyl Cyclase Catalytic Domain Is Involved in NO Activation. Free Radic. Biol. Med 2021, 162, 450–460. 10.1016/j.freeradbiomed.2020.11.001. [PubMed: 33161042]

(17). Zhao Y; Brandish PE; Ballou DP; Marletta MA A Molecular Basis for Nitric Oxide Sensing by Soluble Guanylate Cyclase. Proc. Natl. Acad. Sci 1999, 96 (26), 14753–14758. 10.1073/pnas.96.26.14753. [PubMed: 10611285]

(18). Hall CN; Garthwaite J What Is the Real Physiological NO Concentration in Vivo? Nitric Oxide 2009, 21 (2), 92–103. 10.1016/j.niox.2009.07.002. [PubMed: 19602444]

(19). Ko F-N; Wu C-C; Kuo S-C; Lee F-Y; Teng C-M YC-1, a Novel Activator of Platelet Guanylate Cyclase. Blood 1994, 84 (12), 4226–4233. 10.1182/blood.V84.12.4226. [PubMed: 7527671]

(20). Friebe A; Schultz G; Koesling D Sensitizing Soluble Guanylyl Cyclase to Become a Highly CO-Sensitive Enzyme. EMBO J. 1996, 15 (24), 6863–6868. 10.1002/j.1460-2075.1996.tb01078.x. [PubMed: 9003762]

(21). Stasch J-P; Becker EM; Alonso-Alija C; Apeler H; Dembowsky K; Feurer A; Gerzer R; Minuth T; Perzborn E; Pleiß U; Schröder H; Schroeder W; Stahl E; Steinke W; Straub A; Schramm M NO-Independent Regulatory Site on Soluble Guanylate Cyclase. Nature 2001, 410 (6825), 212–215. 10.1038/35065611. [PubMed: 11242081]

(22). Nakai T; Perl NR; Barden TC; Carvalho A; Fretzen A; Germano P; Im G-YJ; Jin H; Kim C; Lee TW-H; Long K; Moore J; Rohde JM; Sarno R; Segal C; Solberg EO; Tobin J; Zimmer DP; Currie MG Discovery of IWP-051, a Novel Orally Bioavailable SGC Stimulator with Once-Daily Dosing Potential in Humans. ACS Med. Chem. Lett 2016, 7 (5), 465–469. 10.1021/acsmedchemlett.5b00479. [PubMed: 27190594]

(23). Tobin JV; Zimmer DP; Shea C; Germano P; Bernier SG; Liu G; Long K; Miyashiro J; Ranganath S; Jacobson S; Tang K; Im G-YJ; Sheppeck J; Moore JD; Sykes K; Wakefield J; Sarno R; Banijamali AR; Profy AT; Milne GT; Currie MG; Masferrer JL Pharmacological Characterization of IW-1973, a Novel Soluble Guanylate Cyclase Stimulator with Extensive Tissue Distribution, Antihypertensive, Anti-Inflammatory, and Antifibrotic Effects in Preclinical Models of Disease. J. Pharmacol. Exp. Ther 2018, 365 (3), 664–675. 10.1124/jpet.117.247429. [PubMed: 29643251]

(24). Buys ES; Zimmer DP; Chickering J; Graul R; Chien YT; Profy A; Hadcock JR; Masferrer JL; Milne GT Discovery and Development of next Generation SGC Stimulators with Diverse Multidimensional Pharmacology and Broad Therapeutic Potential. Nitric Oxide 2018, 78, 72–80. 10.1016/j.niox.2018.05.009. [PubMed: 29859918]

(25). Wedel B; Humbert P; Harteneck C; Foerster J; Malkewitz J; Bohme E; Schultz G; Koesling D Mutation of His-105 in the B1 Subunit Yields a Nitric Oxide-Insensitive Form of Soluble Guanylyl Cyclase. Proc. Natl. Acad. Sci 1994, 91, 2592–2596. [PubMed: 7908439]

(26). Zhao Y; Marletta MA Localization of the Heme Binding Region in Soluble Guanylate Cyclase. Biochemistry 1997, 36 (50), 15959–15964. 10.1021/bi971825x. [PubMed: 9398330]

(27). Zhao Y; Schelvis JPM; Babcock GT; Marletta MA Identification of Histidine 105 in the B1 Subunit of Soluble Guanylate Cyclase as the Heme Proximal Ligand. Biochemistry 1998, 37 (13), 4502–4509. 10.1021/bi972686m. [PubMed: 9521770]

(28). Koglin M; Behrends S A Functional Domain of the A1 Subunit of Soluble Guanylyl Cyclase Is Necessary for Activation of the Enzyme by Nitric Oxide and YC-1 but Is Not Involved in Heme Binding. J. Biol. Chem 2003, 278 (14), 12590–12597. 10.1074/jbc.M212740200. [PubMed: 12560334]

(29). Kang Y; Liu R; Wu J-X; Chen L Structural Insights into the Mechanism of Human Soluble Guanylate Cyclase. Nature 2019, 574 (7777), 206–210. 10.1038/s41586-019-1584-6. [PubMed: 31514202]

(30). Horst BG; Yokom AL; Rosenberg DJ; Morris KL; Hammel M; Hurley JH; Marletta MA Allosteric Activation of the Nitric Oxide Receptor Soluble Guanylate Cyclase Mapped by Cryo-Electron Microscopy. eLife 2019, 8, e50634. 10.7554/eLife.50634. [PubMed: 31566566]

(31). Campbell MG; Underbakke ES; Potter CS; Carragher B; Marletta MA Single-Particle EM Reveals the Higher-Order Domain Architecture of Soluble Guanylate Cyclase. Proc. Natl. Acad. Sci 2014, 111 (8), 2960–2965. 10.1073/pnas.1400711111. [PubMed: 24516165]

(32). Weichsel A; Kievenaar JA; Curry R; Croft JT; Montfort WR Instability in a Coiled-coil Signaling Helix Is Conserved for Signal Transduction in Soluble Guanylyl Cyclase. Protein Sci. Publ. Protein Soc 2019, 28 (10), 1830–1839. 10.1002/pro.3707.

(33). Childers KC; Yao X-Q; Giannakoulias S; Amason J; Hamelberg D; Garcin ED Synergistic Mutations in Soluble Guanylyl Cyclase (SGC) Reveal a Key Role for Interfacial Regions in the SGC Activation Mechanism. J. Biol. Chem 2019, 294 (48), 18451–18464. 10.1074/jbc.RA119.011010. [PubMed: 31645439]

(34). Liu R; Kang Y; Chen L Activation Mechanism of Human Soluble Guanylate Cyclase by Stimulators and Activators. Nat. Commun 2021, 12 (1), 5492. 10.1038/s41467-021-25617-0. [PubMed: 34535643]

(35). Wittenborn EC; Marletta MA Structural Perspectives on the Mechanism of Soluble Guanylate Cyclase Activation. Int. J. Mol. Sci 2021, 22 (11), 5439. 10.3390/ijms22115439. [PubMed: 34064029]

(36). Jumper J; Evans R; Pritzel A; Green T; Figurnov M; Ronneberger O; Tunyasuvunakool K; Bates R; Žídek A; Potapenko A; Bridgland A; Meyer C; Kohl SAA; Ballard AJ; Cowie A; Romera-Paredes B; Nikolov S; Jain R; Adler J; Back T; Petersen S; Reiman D; Clancy E; Zielinski M; Steinegger M; Pacholska M; Berghammer T; Bodenstein S; Silver D; Vinyals O; Senior AW; Kavukcuoglu K; Kohli P; Hassabis D Highly Accurate Protein Structure Prediction with AlphaFold. Nature 2021, 596 (7873), 583–589. 10.1038/s41586-021-03819-2. [PubMed: 34265844]

(37). Mirdita M; Schütze K; Moriwaki Y; Heo L; Ovchinnikov S; Steinegger M ColabFold: Making Protein Folding Accessible to All. Nat. Methods 2022, 19 (6), 679–682. 10.1038/s41592-022-01488-1. [PubMed: 35637307]

(38). Hu X; Murata LB; Weichsel A; Brailey JL; Roberts SA; Nighorn A; Montfort WR Allostery in Recombinant Soluble Guanylyl Cyclase from *Manduca Sexta*. J. Biol. Chem 2008, 283 (30), 20968–20977. 10.1074/jbc.M801501200. [PubMed: 18515359]

(39). Acerbo AS; Cook MJ; Gillilan RE Upgrade of MacCHESS Facility for X-Ray Scattering of Biological Macromolecules in Solution. J. Synchrotron Radiat 2015, 22 (Pt 1), 180–186. 10.1107/S1600577514020360. [PubMed: 25537607]

(40). Skou S; Gillilan RE; Ando N Synchrotron-Based Small-Angle X-Ray Scattering of Proteins in Solution. Nat. Protoc 2014, 9 (7), 1727–1739. 10.1038/nprot.2014.116. [PubMed: 24967622]

(41). Hopkins JB; Gillilan RE; Skou S BioXTAS RAW: Improvements to a Free Open-Source Program for Small-Angle X-Ray Scattering Data Reduction and Analysis. J. Appl. Crystallogr 2017, 50 (5), 1545–1553. 10.1107/S1600576717011438. [PubMed: 29021737]

(42). Svergun DI Determination of the Regularization Parameter in Indirect-Transform Methods Using Perceptual Criteria. J. Appl. Crystallogr 1992, 25 (4), 495–503. 10.1107/S0021889892001663.

(43). Evers TH; van Dongen EMWM; Faesen AC; Meijer EW; Merkx M Quantitative Understanding of the Energy Transfer between Fluorescent Proteins Connected via Flexible Peptide Linkers. Biochemistry 2006, 45 (44), 13183–13192. 10.1021/bi061288t. [PubMed: 17073440]

(44). van Rosmalen M; Krom M; Merkx M Tuning the Flexibility of Glycine-Serine Linkers To Allow Rational Design of Multidomain Proteins. Biochemistry 2017, 56 (50), 6565–6574. 10.1021/acs.biochem.7b00902. [PubMed: 29168376]

(45). Reddy Chichili VP; Kumar V; Sivaraman J Linkers in the Structural Biology of Protein–Protein Interactions. Protein Sci. 2013, 22 (2), 153–167. 10.1002/pro.2206. [PubMed: 23225024]

(46). Buel GR; Walters KJ Can AlphaFold2 Predict the Impact of Missense Mutations on Structure? Nat. Struct. Mol. Biol 2022, 29 (1), 1–2. 10.1038/s41594-021-00714-2. [PubMed: 35046575]

(47). Martin E; Sharina I; Kots A; Murad F A Constitutively Activated Mutant of Human Soluble Guanylyl Cyclase (SGC): Implication for the Mechanism of SGC Activation. Proc. Natl. Acad. Sci 2003, 100 (16), 9208–9213. 10.1073/pnas.1633590100. [PubMed: 12883009]

(48). Truebestein L; Leonard TA Coiled-coils: The Long and Short of It. BioEssays 2016, 38 (9), 903–916. 10.1002/bies.201600062. [PubMed: 27492088]

(49). Mason JM; Arndt KM Coiled Coil Domains: Stability, Specificity, and Biological Implications. ChemBioChem 2004, 5 (2), 170–176. 10.1002/cbic.200300781. [PubMed: 14760737]

(50). Fritz BG; Hu X; Brailey JL; Berry RE; Walker FA; Montfort WR Oxidation and Loss of Heme in Soluble Guanylyl Cyclase from *Manduca Sexta*. Biochemistry 2011, 50 (26), 5813–5815. 10.1021/bi200794c. [PubMed: 21639146]

(51). Surmeli NB; Marletta MA Insight into the Rescue of Oxidized Soluble Guanylate Cyclase by the Activator Cinaciguat. ChemBioChem 2012, 13 (7), 977–981. 10.1002/cbic.201100809. [PubMed: 22474005]
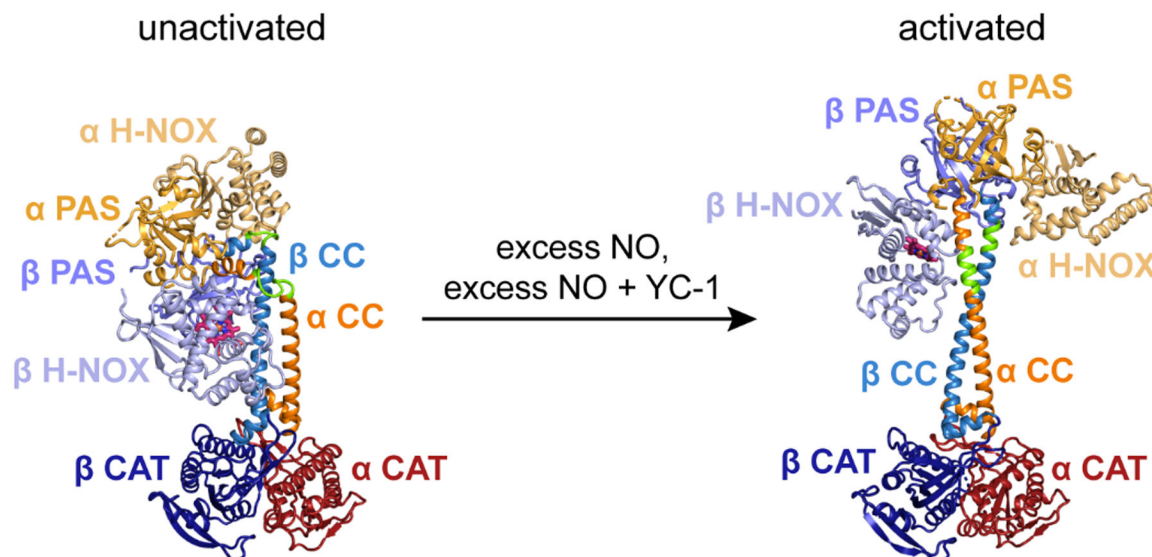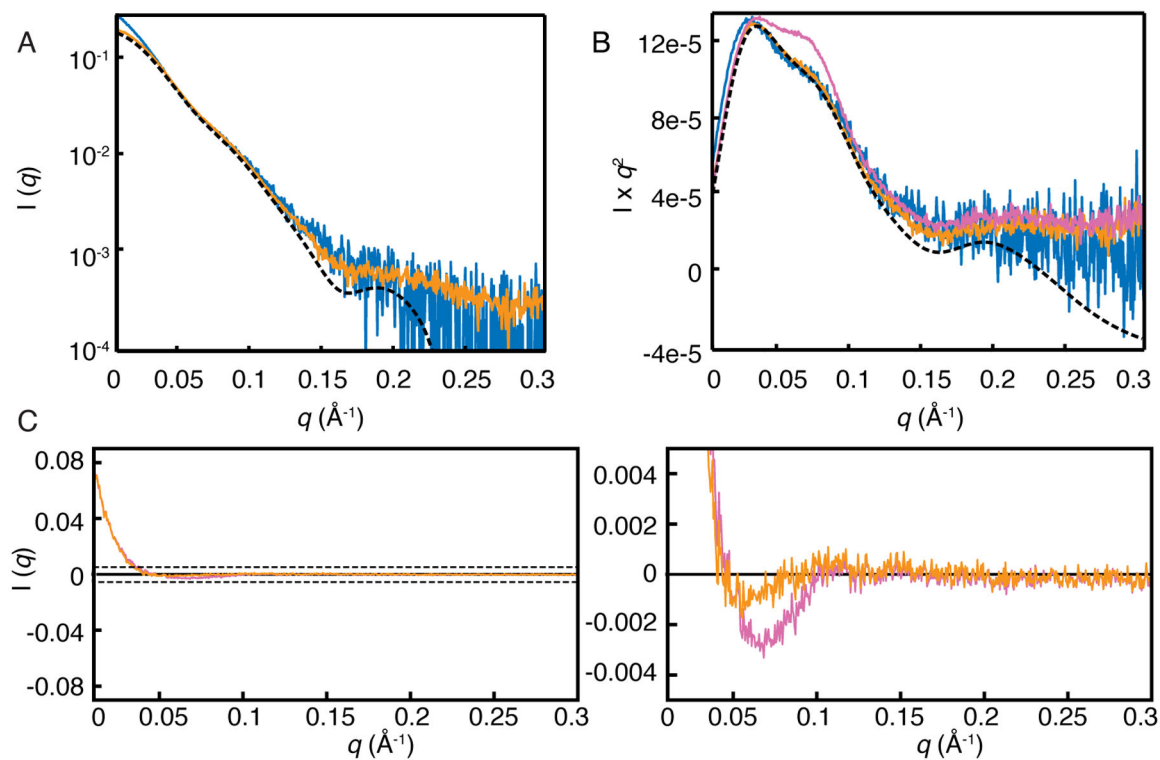
Figure 1.
sGC undergoes a large-scale conformational change upon activation. Protein is shown in ribbon representation and colored by domain. The regions of the CC domains that straighten upon activation are highlighted in green. Heme is shown as sticks with C in pink, N in blue, O in red, and Fe in orange. PDB IDs: 6JT0 (unactivated) and 6JT2 (activated).[29]
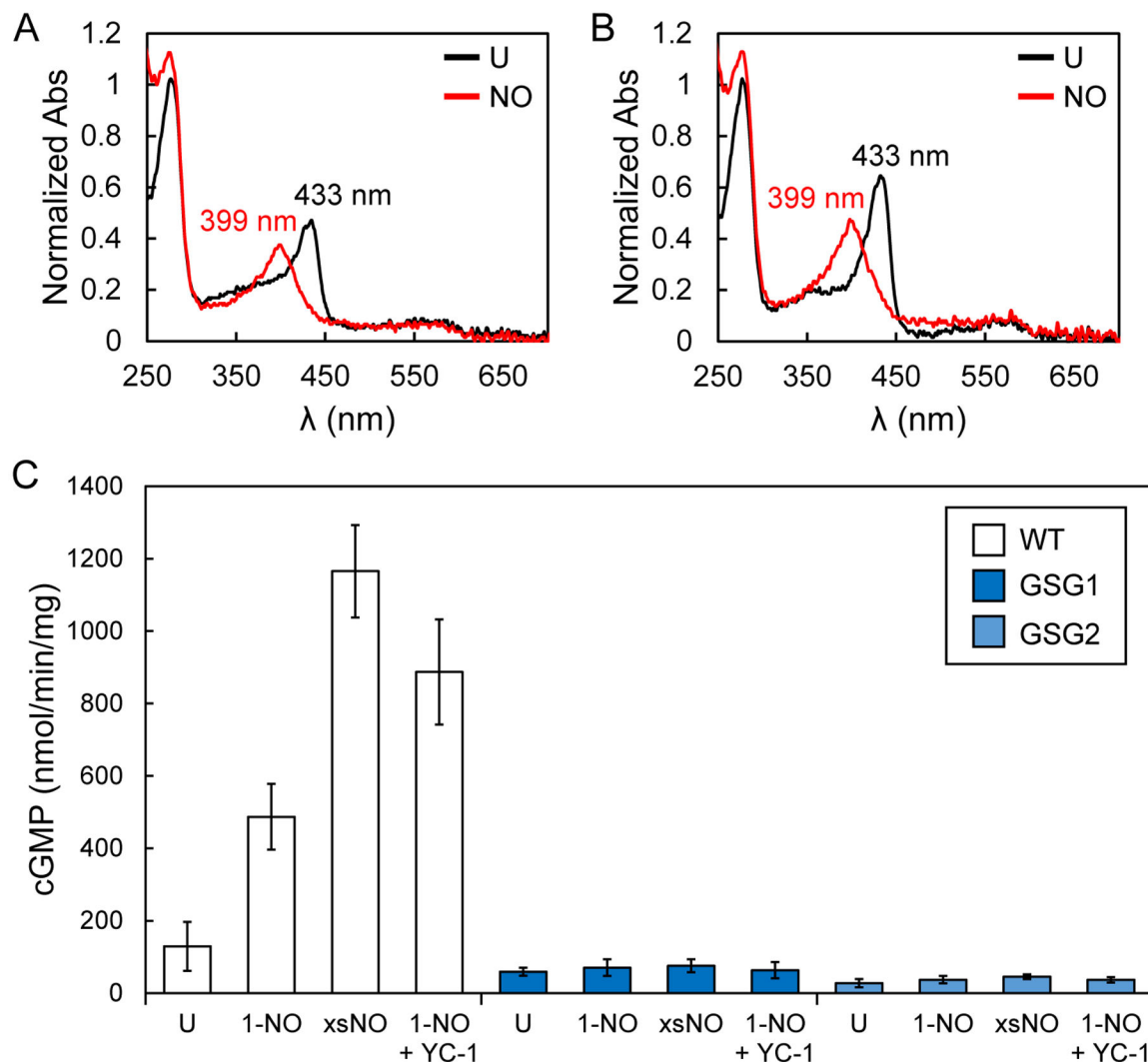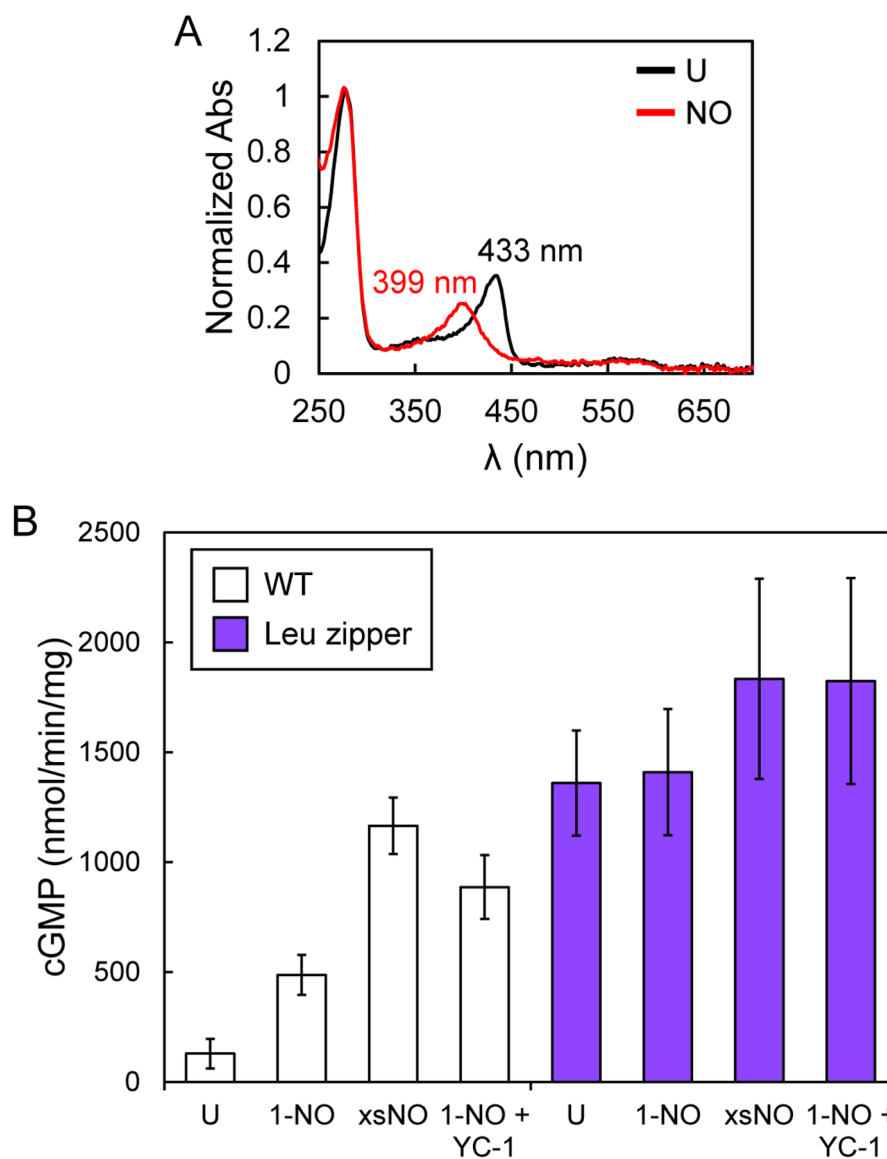
Figure 2.
Characterization of *Ms* sGC(GSG1) and *Ms* sGC(GSG2). A) UV-Vis absorption spectra of *Ms* sGC(GSG1). $A_{433}/A_{280} = 0.47$, ~55% holo protein. B) UV-Vis absorption spectra of *Ms* sGC(GSG2). $A_{433}/A_{280} = 0.64$, ~75% holo protein. C) Activity profiles of the two variants compared to WT. Average specific activities were calculated per mg of holo protein and error bars reflect one standard deviation (n = 3–4).
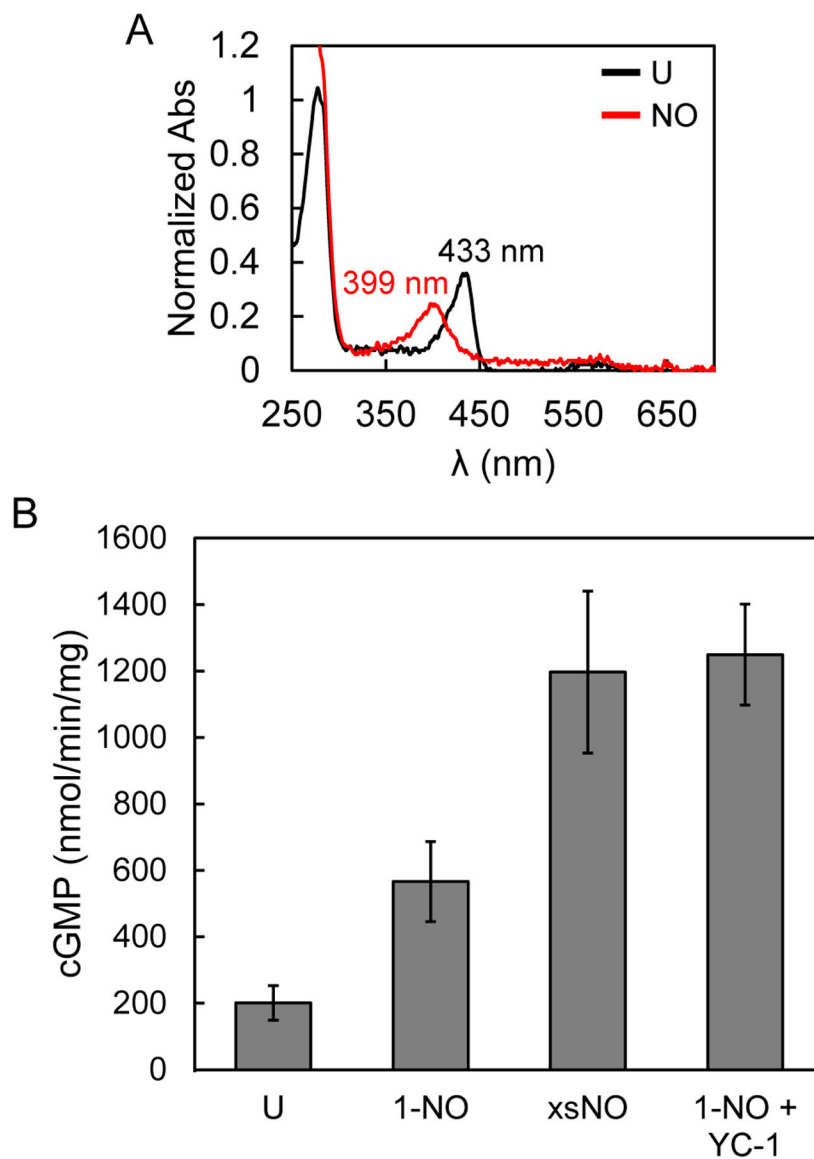
Figure 3.
SAXS results with *Ms* sGC(GSG2). Results are consistent with a well-folded protein in an unactivated, bent conformation. A) Semi-log SAXS profiles of *Ms* sGC(GSG2) unliganded (blue), WT unliganded *Ms* sGC (orange, from ref. 30), and the calculated scattering of the unactivated WT *Ms* sGC cryo-EM structure (black dotted, 6PAS from ref. 30). Differences in scattering at low-*q* are due to aggregation of sample. B) The same profiles are shown in a Kratky plot to better emphasize shared mid-*q* features (blue and orange solid, black dotted). Additionally, the SAXS profile of sGC with 1-NO bound is shown with a pronounced increase in mid-*q* scattering (pink, from ref. 30). C) Difference scattering between *Ms* sGC(GSG2) unliganded and either WT unliganded sGC (orange) or WT NO sGC (pink). The difference scattering is dominated by low-*q* aggregation (*left panel*), but a zoomed view (*right panel*) reveals that WT unliganded sGC is a better match at *q*~0.075 Å.

Figure 4.
Characterization of *Ms* sGC(Leu zipper). A) UV-Vis absorption spectra. $A_{433}/A_{280} = 0.35$, ~41% holo protein. B) Activity profile of the variant compared to WT. Average specific activities were calculated per mg of total protein and error bars reflect one standard deviation (n = 3).

Figure 5.
Characterization of heme-deficient WT *Ms* sGC. A) UV-Vis absorption spectra. $A_{433}/A_{280} = 0.33$. B) Activity profile of the sample. Average specific activities were calculated per mg of holo protein and error bars reflect one standard deviation (n = 3).